Surface textures suppress viscoelastic braking on soft substrates

Martin Coux[a,1] and John M. Kolinski[a,1]

[a]Engineering Mechanics of Soft Interfaces, School of Engineering, École polytechnique fédérale de Lausanne, 1015 Lausanne, Switzerland

Edited by Laurent Limat, Centre national de la recherche scientifique, Paris, France, and accepted by Editorial Board Member John D. Weeks October 28, 2020 (received for review May 7, 2020)

A gravity-driven droplet will rapidly flow down an inclined substrate, resisted only by stresses inside the liquid. If the substrate is compliant, with an elastic modulus $G < 100$ kPa, the droplet will markedly slow as a consequence of viscoelastic braking. This phenomenon arises due to deformations of the solid at the moving contact line, enhancing dissipation in the solid phase. Here, we pattern compliant surfaces with textures and probe their interaction with droplets. We show that the superhydrophobic Cassie state, where a droplet is supported atop air-immersed textures, is preserved on soft textured substrates. Confocal microscopy reveals that every texture in contact with the liquid is deformed by capillary stresses. This deformation is coupled to liquid pinning induced by the orientation of contact lines atop soft textures. Thus, compared to flat substrates, greater forcing is required for the onset of drop motion when the soft solid is textured. Surprisingly, droplet velocities down inclined soft or hard textured substrates are indistinguishable; the textures thus suppress viscoelastic braking despite substantial fluid–solid contact. High-speed microscopy shows that contact line velocities atop the pillars vastly exceed those associated with viscoelastic braking. This velocity regime involves less deformation, thus less dissipation, in the solid phase. Such rapid motions are only possible because the textures introduce a new scale and contact-line geometry. The contact-line orientation atop soft pillars induces significant deflections of the pillars on the receding edge of the droplet; calculations confirm that this does not slow down the droplet.

elastocapillarity | soft matter | droplets | polymers

From the raindrops pendent on a window to the fog on humid glasses, liquid droplets often get stuck on solid surfaces, even when those surfaces are vertical. Such retention of liquids arises due to microscopic heterogeneities of the substrate that pin the liquid–solid contact line in place (1); the pinning strength can be measured by contact-angle hysteresis (2, 3), that is the difference between the advancing and trailing contact angle for a droplet at the onset of motion over a solid surface. The pinning of droplets on substrates is often undesirable, as it can lead to proliferation of microorganisms, corrosion, or degradation of optical properties for transparent materials including solar cells and reflectors. Contact line pinning is essentially nonexistent on soft materials––they exhibit very low contact-angle hysteresis (4, 5). At the three-phase juncture, a soft solid forms a wetting ridge (6), resulting from the equilibrium of capillary stresses at the contact line and elastic stresses in the material. For a substrate with shear modulus G, a liquid of surface tension γ induces the formation of a ridge of typical dimension $\gamma/2G$, proportional to the elastocapillary length of the solid $\gamma_s/2G$ (where γ_s is the surface tension of the gel). The consequences of this deformation are substantial for contact-line dynamics, as the ridge induces stick–slip motion (7, 8), self-propulsion of droplets (9), and long-range interactions between droplets (10).

The contact line advances by surfing the elastocapillary ridge (11), which moves in tandem with the liquid; the microscopic liquidlike behavior of soft solids drastically reduces contact-line pinning at their top. However, the motion of the solid corner leads to substantial viscous dissipation in the solid phase (12, 13), slowing down the drop, which rarely translates faster than a few micrometers per second, an effect called "viscoelastic braking." Hence, even if the drop is not "sticking" to the material, it is essentially dynamically pinned, because its low velocity will result in long residence times on the substrate, potentially leading to the same fouling problems that arise for pinned droplets. Studies of the dynamics of the three-phase contact line on soft solids provide insight on how to reduce this effect, as the viscous dissipation has been shown to be dependent on the speed of the contact line (11) and the thickness (14) of the soft substrate. However, no solution has been proposed to fully suppress viscoelastic braking.

Here, we study the effect of decorating soft silicone gels of storage modulus of order kPa with 100-μm textures on their wetting properties. Texturing solids at scales ranging from hundreds of nanometers to hundreds of micrometers change their wetting properties, making hydrophilic solids more hydrophilic and hydrophobic ones more hydrophobic (15). On densely textured hydrophobic substrates, air can be trapped below water or other liquids with high surface tension (16), that are in the superhydrophobic Cassie state. Such substrates are water-repellent (17), self-cleaning (18), and can even reduce drag (19). In this state, droplets move much faster than on smooth substrates, due to the combination of high contact angles and weak pinning (20, 21). We show that the Cassie state on soft textured substrates is qualitatively different from that on hard textured solids; the multiple triple lines below a droplet are deformed by surface tension. Using confocal microscopy, we show that every texture beneath the droplet is decorated

Significance

The transport of liquids on solid substrates is ubiquitous in our daily experience, and vital to many industrial and fundamental processes. Enabled by surface texturing and chemical treatment, engineers have recently developed methods to enhance liquid motion over rigid surfaces. With increasing applicability of soft materials, the motion of liquids over soft substrates has become important, especially in medical settings. Indeed, elastocapillary phenomena profoundly alter liquid transport over such soft surfaces due to substrate deformation, leading to enormous resistance to liquid motion over the surface, and thus enabling harmful fouling effects. Here we show that surface texturing on compliant substrates leads to giant suppression of this viscoelastic braking phenomenon, facilitating droplet motion over compliant surfaces.

Author contributions: M.C. and J.M.K. designed research; M.C. performed research; M.C. and J.M.K. analyzed data; and M.C. and J.M.K. wrote the paper.

The authors declare no competing interest.

This article is a PNAS Direct Submission. L.L. is a guest editor invited by the Editorial Board.

[1]To whom correspondence may be addressed. Email: martin.coux@epfl.ch or john.kolinski@epfl.ch.

This article contains supporting information online at https://www.pnas.org/lookup/suppl/doi:10.1073/pnas.2008683117/-/DCSupplemental.

First published December 4, 2020.

with a wetting ridge in a plane parallel to the substrate. Despite the existence of these multiple elastocapillary deformations, we show that viscoelastic braking is suppressed on soft textured substrates, and the dominant resistance to their motion is the liquid's viscosity; indeed, the viscous dissipation in the solid is not observed to play a role. Based on high-speed imaging of the microscopic contact lines at the top of the peripheral textures below a droplet, we identify the mechanisms responsible for the suppression of viscoelastic braking. We finally show that the suppression of the dissipation in the solid phase comes with a price, as decorating soft substrates with textures induces retention of liquid, in contrast to what is observed on hard substrates, where texturing usually reduces pinning.

Materials and Methods

We produce ultrasoft textured substrates using established replication techniques from a master substrate. We first produce a silicon wafer covered with cylindrical pillars of height 93 ± 0.5 μm, radius 50 ± 0.5 μm, arrayed on a square lattice with a pitch of 200 ± 0.5 μm; the corresponding solid fraction ϕ is 20%. The wafer is chemically treated with trichloroperfluorooctylsilane (Sigma-Aldrich) via chemical vapor deposition and molded with polydimethylsiloxane (PDMS) Sylgard 184 (Dow Corning), cured at 80 °C for 4 h. The PDMS mold is in turn silanized with the same process and filled with Dow Corning CY52-276 A/B in proportions 1:1.2, dyed with 1% of fluorescent dye (TP-3400, Tracer Products). The ensemble is then covered with a 150-μm-thick microscope slide, separated from the PDMS mold by two 170-μm cover slides used as spacers, and put into an oven at 70 °C for 15 min. At the end of the curing process, the textured substrate is extracted from the mold. The silicone gel has a shear modulus $G = 2.36 \pm 0.15$ kPa (*SI Appendix*, Fig. S1). Using optical microscopy to image the substrate from both the top and the side, we verify the fidelity of the replication process by measuring the geometry of the textures, as shown in Fig. 1*A*. Within the resolution of our image, the shape and geometry of our replica match those of our master substrate.

The hydrophobic silicone gel is rendered superhydrophobic by the addition of textures; liquids with high surface tension can thus be maintained at the top of the surface features. A 20 μL droplet of glycerol (density $\rho = 1.26 \pm 0.01$, surface tension $\gamma = 63.4 \pm 0.2$ mN/m, viscosity $\eta = 1120 \pm 40$ mPa·s, Sigma-Aldrich) deposited on the ultrasoft textured substrate exhibits a high contact angle (151 ± 2°, Fig. 1*B*) and is weakly pinned (the liquid rolls off the substrate when inclined by 14 ± 0.5°), as expected for a liquid in the superhydrophobic Cassie state.

In order to probe the static elastocapillary interactions with a smooth soft substrate, we retain untextured millimetric patches adjacent to the textures, as sketched in Fig. 1*C*, *Top*. On such a patch, we deposit a millimetric droplet of glycerol dyed with 1% blue alimentary dye (Jolly dessert, Migros) fluorescing at wavelengths between 700 and 800 nm when excited at 633 nm. Glycerol is poorly wetting on the silicone gel: the droplet adopts a hemispherical shape with contact angle $\theta = 89 \pm 2°$. Contact-angle hysteresis $\Delta\theta$ is very low, equal to 4 ± 2°. Furthermore, glycerol has an optical index close to that of the silicone gel; for the liquid and the solid, the optical indices are 1.47 and 1.42, respectively. We image the triple line with a Leica SP-8 confocal microscope using a 93× glycerol immersion objective (Leica HC PL APO 93×/numerical aperture, NA, of 1.3). The gel fluoresces between 450 and 600 nm when excited at 405 nm; there is no cross-talk between the fluorescence signals of the solid and the liquid. We use two separate excitation and detection channels and thus resolve the location of the different phases with high precision. Fig. 1*C*, *Bottom* shows the triple line formed by the glycerol (cyan) droplet. The initially flat solid (red) is deformed by the contact line, creating a wetting ridge with a height of 12 ± 0.5 μm, in good agreement with $\gamma/2G = 13.3$ μm, the expected amplitude of deformation for glycerol on the soft silicone gel. At the tip of the corner, the solid forms an angle of 78 ± 3°.

Static Interaction between Drops and Compliant Textured Substrates

The addition of textures fundamentally changes the interactions of the droplet and the soft substrate. In the Cassie state, the droplet is supported by air-permeated textures; the three-phase contact line thus forms at the top of each texture beneath the liquid. However, not all textures are subjected to the same

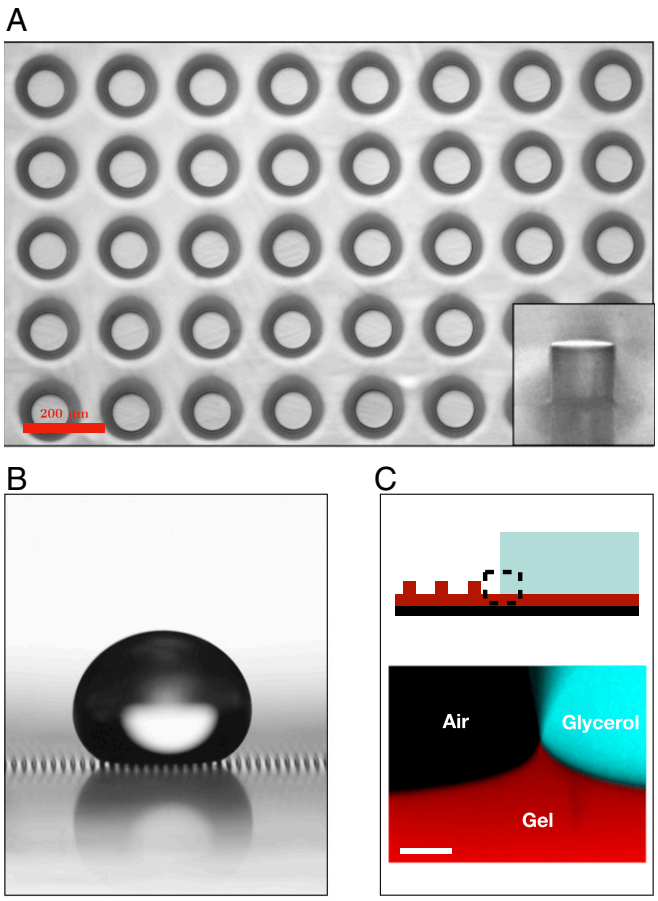

Fig. 1. (*A*) Microscopic top view of an ultrasoft textured substrate. The textures are cylinders of diameter 100 ± 1 μm and height 93 ± 0.5 μm deposited on a square array of pitch 200 ± 0.5 μm. Their aspect ratio and shape can be seen in side views, as shown in inset. (*B*) Picture of a 20 μL glycerol droplet deposited on an ultrasoft textured substrate. The liquid exhibits high contact angle 151 ± 2°, small contact radius, and rolls off the substrate when inclined of 14 ± 0.5°; it is in the superhydrophobic Cassie state. (*C*, *Bottom*) Confocal microscopy observation of a contact line formed when a glycerol fluorescent droplet (cyan) is deposited on a flat region of an ultrasoft textured fluorescent substrate (red), as sketched at top. The initially flat substrate is deformed by the liquid–vapor surface tension, forming a ridge of height 12 ± 0.5 μm at the triple line. (Scale bar, 10 μm.)

capillary stresses, as shown schematically in Fig. 2*A*; the textures can thus be divided into two groups, one along the periphery of the projected contact area and the other internal to this area. At the top of each internal texture, the contact line is symmetric about the pillar's axis, and exerts an isotropic capillary stress in the plane of the surface. Atop the peripheral textures, the capillary stresses are no longer symmetric, and the capillary force exerted by the contact line is not balanced in the horizontal plane. This force results in giant deflections of the soft pillars, as can be seen from the side, as shown in Fig. 2*B*. Here, an initially vertical peripheral pillar is deflected by $\delta = 37 \pm 1$ μm due to the asymmetric contact with glycerol. Elastocapillary deformations on silicone elastomer textured substrates with shear modulus of order MPa have been reported: slender textures bend as a consequence of the asymmetry of the contact lines at their top (22, 23); here, however, the textures have a low aspect ratio and the deformations are comparable to the size of the textures. As a consequence of their aspect ratio, the peripheral textures undergo a deformation consisting of both rigid-body rotation and bending.

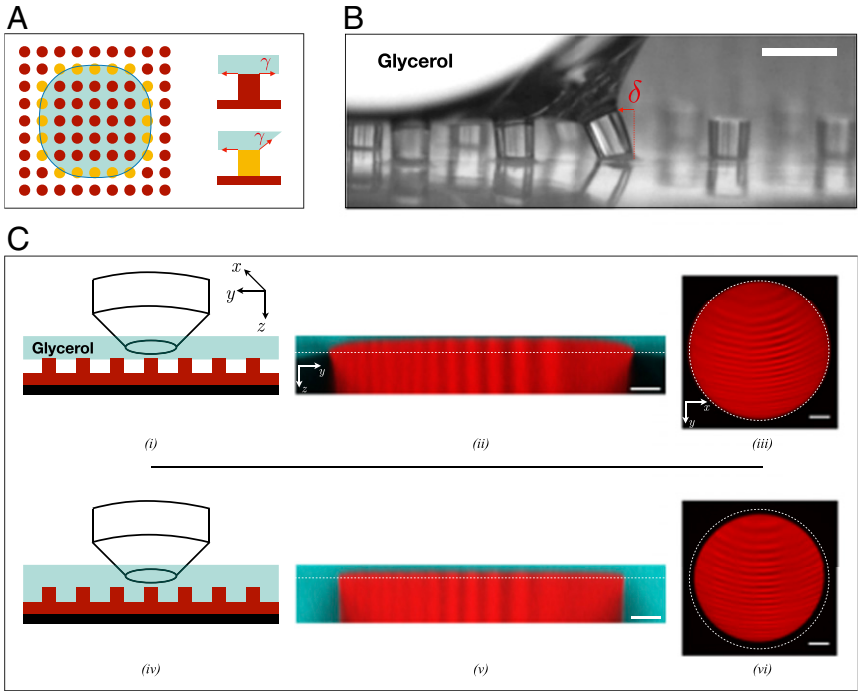

Fig. 2. (*A*) Schematic representation of the contact region of a droplet in the Cassie state on a textured substrate. The pillars internal to the liquid–solid contact are isotropically stressed by capillary forces in the horizontal plane (as sketched in top right corner). In comparison, the pillars at the periphery of the liquid–solid contact (yellow) are subjected to imbalanced capillary forces along the horizontal (bottom right corner). On soft textured substrates, these asymmetric capillary stresses deform the peripheral textures, as shown in the side-view microscopy image in (*B*). The asymmetric capillary stress deflects the central texture by $\delta = 37 \pm 1$ μm. (Scale bar, 200 μm.) (*C*, *i*) A sketch of the confocal setup used to study the soft Cassie state. The immersion fluid (here glycerol) is maintained at the top of the pillars by surface tension. An optical volume is reconstructed around the top of a single pillar. A cut through this volume over a vertical (*y*-*z*) plane passing through the center of the cylinder is shown in *C*, *ii*. The glycerol (cyan) is maintained at the top of the pillar (red). The cylinder radius varies along its height and is maximal at the triple line. The height of the triple line is indicated with the dashed white line. (*C*, *iii*) Horizontal (*x*-*y*) slice of the same pillar at the contact line; the perimeter of the pillar at this height is indicated by the white dashed circle. *C*, *iv*–*vi* show the same confocal setup and observations in the superhydrophobic Wenzel state, when the liquid has penetrated into the textures. The white dashed circle in *C*, *vi* indicates the maximal perimeter in the Cassie state. (All scale bars, 10 μm.) Stripes in the pillar's fluorescent signal arise from interference effect in the excitation field.

The deflection of the peripheral textures is not the only elastocapillary deformation that can be observed below a droplet on a soft textured substrate. In order to image the triple lines formed at the top of every pillar in the Cassie state, we use confocal microscopy with fluorescent glycerol. As sketched in Fig. 2 *C*, *i*, the fluorescent glycerol is used simultaneously as an immersion fluid and as the wetting phase, enabling direct, high-resolution imaging of the liquid-solid contact region at the top of a single pillar.

We reconstruct an optical volume containing the top of a single pillar and the surrounding fluid using images captured with the microscope (Movies S1 and S2). We define an orthonormal coordinate system where axis *z* is parallel to the axis of the pillar (Fig. 2*C*, *i*); Fig. 2*C*, *ii* and 2*C*, *iii* show two slices through this volume in a vertical (*y*-*z*) and horizontal (*x*-*y*) plane. The *x*-*y* plane is imaged at the height corresponding to the position of the contact line, indicated by the dashed line in Fig. 2C, *i*. The glycerol (cyan) remains atop the texture (red) and the air (black) is trapped between the pillar and the liquid, as the liquid is in the Cassie state. The shape of the pillar in the Cassie state is significantly different from that observed in Fig. 1*A*. The pillar indeed does not have a uniform diameter—it is wider at its top, where the triple line sits. At its maximal extent, its diameter is 103 ± 0.5 μm. Furthermore, the top of the cylinder is not flat, but rounded close to its edges, as shown in Fig. 2*C*, *ii*. The solid subtends an angle of $105 \pm 5°$ at the contact line, higher than the angle at the tip of the ridge on flat regions of the same substrate. Both deformations along the *y* axis (extension of the diameter) and *z* (rounding of the top) decay on a similar length of about 15–20 μm.

Because the Cassie state is metastable, an increase in the pressure in the fluid leads to its penetration into the textures (24). The corresponding superhydrophobic state is called the Wenzel state; in this configuration, the triple line at the top of each texture is no longer present, as sketched in Fig. 2*C*, *iv*. We use the objective to pressurize the glycerol and trigger the transition from the Cassie to the Wenzel state. In this way, we can image the same pillar with and without a triple line at its top. Once the textures are fully wetted, we observe that the pillar recovers its shape observed in absence of a contact line at its top: it is cylindrical, as shown in Fig. 2*C*, *v* and Movie S3. Its diameter is 97 ± 0.5 μm, 6 μm smaller than in the Cassie state, as shown by the image and white dashed circle in Fig. 2*C*, *vi*. The ridges on soft textured substrates are oriented horizontally due to the position of the contact line. They have an extension of 3 μm, significantly smaller than those on smooth substrates. This discrepancy could be due to the finite size or curved geometry of the pillar, which causes gradients in the deformations, and thus the strains, to be larger, as reported for ridge sizes in previous works (25). Finally, the solid angle, reported to be independent of drop size and substrate thickness for a given liquid/flat soft substrate (26), is larger when the contact line surrounds the top of a soft pillar. Beneath the projected contact area of the droplet in the Cassie state, the shape of every soft texture element is modified by the multiple triple lines, leading to significant total deformation of the substrate at the top of the textures. The deformation atop each pillar is qualitatively similar to that observed at the triple line on soft flat substrates, which is at the origin of viscoelastic braking. This effect is not observable on

hard substrates: on a textured PDMS substrate with elastic modulus of order 2 MPa, where the elastocapillary length is of order 10 nm, the geometry of the pillar is the same in both superhydrophobic situations (*SI Appendix*, Fig. S2).

Dynamics of Droplet Motion over Soft Textured Substrates. Despite the numerous elastocapillary deformations observed in the static case, the addition of textures on soft substrates dramatically accelerates the motion of droplets. To probe this effect, droplets of glycerol of controlled volume $\Omega = 11.9 \pm 0.1$ μL are gently deposited on either of two soft substrates, with and without textures. The smooth substrates have a constant thickness of 150 μm. The soft surfaces are inclined to the horizontal with an angle α ranging from 0° to 75°, subjecting the droplet to a force $\rho\Omega g \cdot \sin\alpha$. Depending on the surface properties, a critical angle α^* must be exceeded for the droplet to move along the surface. This angle provides a measurement of contact-angle hysteresis because, at the onset of motion, the driving force equals the retention force, i.e., $\rho\Omega g \cdot \sin\alpha^* \sim \gamma\Omega^{1/3}(\cos\theta_r - \cos\theta_a)$, where θ_a and θ_r are the advancing and receding contact angles, respectively (2, 3). On soft smooth substrates, pinning of liquid is absent; the critical angle for the onset of droplet motion is vanishingly small. We indeed observe (very slow) sliding of glycerol droplets on smooth substrates inclined by less than 10°, in stark contrast to what happens on textured substrates, where the liquid—while in the Cassie state—does not slide for inclinations lower than $\alpha^* = 22 \pm 0.5°$, as can be seen from the velocity data displayed in Fig. 3*A*. Textures thus lead to pinning of droplets on the soft substrate, unlike what is observed on hard substrates, where the textures only facilitate droplet motion. On both substrates, the droplets move with constant velocity U after a short transient regime. We measure U via images recorded at fixed rates with a camera (Nikon D850 or Photron Mini-UX 100). The sliding velocities on the textured substrate, observed for inclinations larger than α^*, are higher by four orders of magnitude than on the smooth substrate, ranging from 1 to 20 mm/s. Texturing of soft substrates thus leads to a giant reduction of viscoelastic braking. On soft substrates, U increases with the forcing applied to the droplet; however, the velocity variations are different for textured and smooth substrates, as can be seen in Fig. 3*A*). As predicted by viscoelastic braking (6), on smooth substrates with large and constant thickness (14), U varies as a power-law function of the driving force, $U \propto (\rho\Omega g \cdot \sin\alpha)^{1/n}$, where $n = 0.53$ is determined by the scaling of the loss modulus G'' with shear rate ω as $G''(\omega) \propto \omega^n$ (6, 11) (see rheological measurements in *SI Appendix*, Fig. S1). The data on the textured substrate cannot be described with the same power law; instead, U varies linearly with forcing above α^*: $U \propto \rho\Omega g \cdot (\sin\alpha - \sin\alpha^*)$. The different velocity regimes are demarcated by the color panels in Fig. 3*A*.

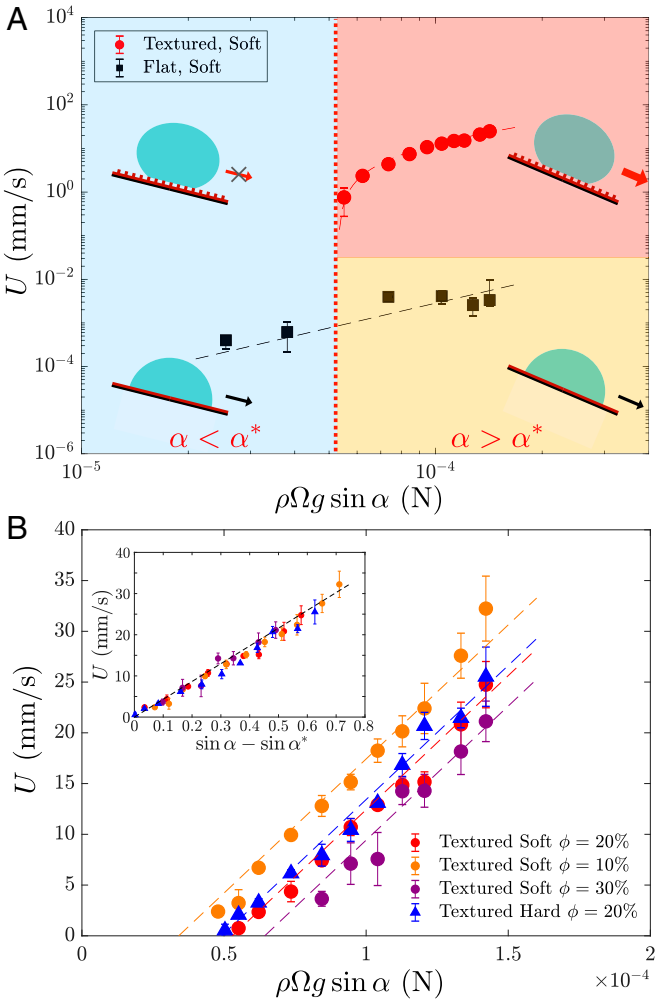

Fig. 3. (*A*) Sliding velocities of a glycerol droplet of volume $\Omega = 11.9$ μL on soft substrates, respectively, flat (black dots) and textured with pillar density 20% (red dots) substrates inclined at an angle α, as a function of its weight projected along the vertical axis. The color panels represent ranges of influence of the textures on the motion dynamics: at low inclinations, below $\alpha^* = 22 \pm 0.5°$ (blue zone), textures induce pinning; above α^* textures suppress viscoelastic braking (red zone) that is observed on flat substrate (yellow zone). The red dashed line shows the best fit of velocity data on textured substrate of type $U \propto \rho\Omega g \cdot (\sin\alpha - \sin\alpha^*)$; the black dashed line shows a power law $U \propto (\rho\Omega g \cdot \sin\alpha)^{1/n}$ where $n = 0.53 \pm 0.02$ is determined from a fit of the rheological measurements, as $G''(\omega) \propto \omega^n$. (*B*) Comparison between sliding velocities of a glycerol droplet of volume $\Omega = 11.9$ μL on textured substrates, either hard (blue triangles) with texture density 20%, or soft with pillar densities 10, 20, and 30% (respectively, orange, red, and purple dots) as a function of the projected weight. The dashed lines are a guide for the eye; all data collapse on a single line of slope 0.043 ± 0.002 m/s ($0.76\frac{\gamma}{\eta}$ for glycerol) when plotted as a function of $\sin\alpha - \sin\alpha^*$ (*Inset*).

Downloaded at Palestinian Territory, occupied on December 27, 2021

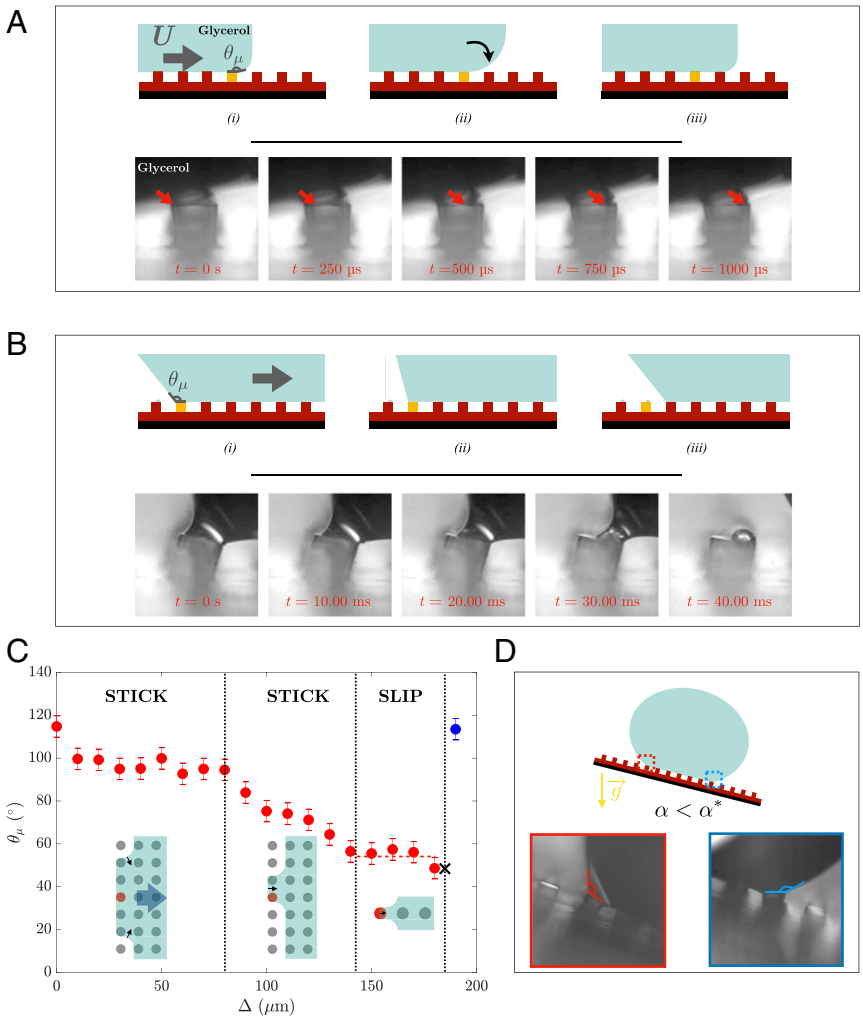

Fig. 4. (*A, Top*) Schematic representation of contact-line progress on the advancing side in the Cassie state. As the bulk of the droplet advances with velocity *U* (*A*, *i–ii*), the triple line at the top of the frontmost pillar (yellow) bends and the microscopic contact angle at its top θ_μ increases until liquid–solid contact occurs on the next dry pillar (between *A*, *ii* and *A*, *iii*). Once liquid–solid contact initiates on the next dry pillar, it is totally wetted in 1 ms, as shown in the time series in *A*, *Bottom*, where *U*= 1 mm/s and red arrows indicate the position of the triple line. (*B*, Top) Schematic representation of the contact line receding in the Cassie state. As the bulk of the droplet moves away from the pillar with velocity U (*B*, *i–ii*), the liquid–air interface bends until θ_μ reaches a critical value. The liquid then sweeps over the top of the trailing pillar and deposits a tiny droplet at its top when detaching from it between instants *B*, *ii* and *B*, *iii*. Contact-line motion occurs during less than 40 ms, as shown in the time-lapse series in *B*, *Bottom* where $U = 1$ mm/s. (*C*) Microscopic contact angle θ_μ at the top of a trailing texture (sketched in red, *Inset*) as a function of Δ, the bulk displacement of the droplet, as it translates at 1 mm/s. $\Delta = 0$ is taken at the depinning from the previous pillar; the black dotted lines show the transitions between the different depicted regimes described in the text. The contact line remains stuck on the red pillar and starts sliding with constant θ_μ only when it reaches 55 ± 2°, as indicated with the red dashed line. The black cross indicates the instant of depinning. The last reported angle (blue point) is measured at the top of the next pillar, and the cycle repeats. (*D*) As sketched in the top half, we zoom on the receding (red) and advancing (blue) side of a 11.9 µL glycerol droplet stuck on a soft textured substrate inclined at 20°, below α^*. The contacts at the top of the textures are displayed in the bottom half of the panel; the microscopic contact angles θ_μ are equal to 119 ± 2° on the receding side and 148 ± 2° on the advancing side.

textured substrates (28). However, it does not change significantly with substrate compliance; with $\phi = 20\%$, the pinning is only slightly stronger on soft textured substrates than on hard ones. Furthermore, the variation of pinning force on soft substrates with texture density is in good agreement with the expected scaling from (28): $\rho\Omega g \sin\alpha^* \sim \phi \log(\pi/\phi)$ (*SI Appendix*, Fig. S3). Upon accounting for pinning, all data collapse on a single line and follow the linear relationship expected for large viscous droplets on hard textured substrates, $U \propto \frac{\gamma}{\eta}(\sin\alpha - \sin\alpha^*)$ (29) with a prefactor close to unity, 0.76 ± 0.03, as shown in inset of Fig. 3*B*. Although water droplets cannot reach their terminal velocity on the length of soft textured substrates, similar results can be obtained with liquids of intermediate viscosities. In *SI Appendix*, Fig. S4, we report the terminal velocities reached by droplets comprising water and glycerol with viscosity 165 ± 10 mPa·s on soft and hard textured substrates. The data obtained on both substrates with these other fluids are also simply shifted due to a slight change in pinning strength. These results underscore that the main resistance to droplet motion on soft textured substrates remains viscous dissipation in the liquid phase [scaling with the viscosity (27)], even for fluids almost 10× less viscous than pure glycerol. Textures thus screen viscoelastic dissipation in the solid phase.

To understand the profound difference in dynamics induced by textures, we probe the dynamics of a moving glycerol droplet on a soft textured substrate using direct high-speed microscopy to image the liquid–solid contact line at the advancing and receding edges of the droplet. As reported in previous studies (30, 31),

contact-line motions are restricted to the texture elements at the periphery of the contact area while all texture elements internal to the contact area remain unaffected by the motion of the droplet; we thus do not expect the internal textures to play a role in the dynamics of moving droplets despite their substantial deformation. The periphery of the contact area is maintained within the field of view of our microscope by holding the droplet stationary using a needle and displacing the substrate with a linear actuator. After bringing the liquid into contact with the solid, the substrate is set into motion at controlled speed $U = 1$ mm/s using a programmable linear actuator (Newport LTA-HS).

The global motion of the droplet leads to a repetition of pinning and depinning events from one pillar to the next at its peripheral edges, as shown schematically in the top halves of Fig. 4 *A* and *B* and Movies S4 and S5. On both edges, the contact line remains pinned, forming a microscopic contact angle θ_μ at the top of the textures, that we measure from the side at the scale of a single texture; θ_μ is different from the macroscopic advancing and receding angles usually measured at the scale of the drop (31, 32). As the droplet moves relative to the pillar, the liquid–air interface deforms. On the advancing side, the liquid–solid interface bends, causing θ_μ to increase until contact initiates on the next texture, completing the cycle. On the receding edge, θ_μ decreases, causing progressive bending of the pillar, until the contact line dewets from the pillar and jumps to the next one. After liquid detachment, the pillar relaxes in about 10 ms. These events repeat cyclically, on average every $T = 200$ ms, a period set by the ratio between the texture pitch and the substrate velocity. This repetitive and macroscopically smooth motion is punctuated by discontinuous events when the contact line is set into rapid motion at both the advancing and receding edges. At the advancing edge, the top of the next pillar is completely wetted within 1 ms after liquid–solid contact initiates, as shown in Fig. 4*A*, *Bottom*. During the wetting of the pillar, the contact line thus advances at an average velocity of ~10 cm/s, much higher than the velocity of the bulk droplet. For the remainder of *T*, the contact line remains pinned at the top of the pillar while the bulk of the droplet advances. At the receding edge, the motion occurs after a critical distortion of the contact line, the liquid then dewets from the pillar within 40 ms, as shown in Fig. 4*B*, *Bottom*, moving with an average velocity of order 1 mm/s, comparable to *U*. For the remainder of *T*, the liquid is pinned at the top of the pillar and the motion of the droplet is mediated by variations of the microscopic contact angle θ_μ that does not lead to contact line motion. The experiment was repeated for stage velocities varied between 1 and 10 mm/s and we observed similar behaviors at both advancing and receding edges of the droplet; only the dewetting events on the trailing edge occur faster as *U* is larger.

Along the perimeter of a moving droplet in the Cassie state on a soft textured substrate, despite the existence of wetting ridges at every liquid–solid contact, the microscopic contact lines at the top of the textures thus move at velocities significantly larger than allowed by viscoelastic braking, observed on flat soft substrates, and that are at higher forcing of 10 μm/s. This is a consequence of the conformation of the multiple triple lines sitting on the peripheral pillars. On the advancing side, the liquid is pinned on the peripheral pillars; contact-line motions occur only when liquid touches the following texture. The initiation of liquid–solid contact on the next pillar resembles the initiation of the contact between a pendant viscous droplet and a flat substrate, where the contact-line dynamics are controlled by the liquid viscosity (33), and spreading is shown to be independent of substrate compliance during the first milliseconds (34, 35). We thus expect viscous losses in the solid to be negligible compared to those in the liquid. The motions are qualitatively different on the receding side of the droplet: there, the liquid dewets from the pillars. To understand the rapid events in this region, we measure the microscopic contact angle θ_μ at the top of one of the central pillars of the wetted row that forms the receding edge of a moving droplet. This angle decreases as the bulk of the liquid advances by a distance Δ at $U = 1$ mm/s, as shown in Fig. 4*C*; $\Delta = 0$ corresponds to the depinning of the liquid from the previous row. The inset sketches represent the progress of the receding edge as the droplet advances. First, the bulk droplet motion forces the progressive detachment of the contact line, pillar by pillar along a row, starting with the extremal textures in this row (30, 36). For the central pillars in this row, θ_μ remains approximately constant with a value of $97 \pm 4°$. Only when a few pillars remain at the receding edge, θ_μ undergoes a series of transitions, decreasing rapidly until depinning critically when reaching a value of $55 \pm 2°$, which it retains as the contact line sweeps across the top of the texture. Finally, a small droplet pinches off from the fluid bulk and remains at the top of the texture. The bulk of the liquid advances of 150 μm before the rapid motion of the contact line initiates. This global behavior, together with the critical value of θ_μ required to trigger the slipping event, remains unchanged as *U* increases from 1 to 10 mm/s, and when the distance between pillars is varied. For driven fluid motion over flat soft surfaces, dynamical depinning occurs beyond a critical forcing, when the solid undergoes reduced deformation at high forcing rates, leading to limited dissipation in the solid phase (11, 37) and thus, to contact-line motion with velocities set by the dissipation in the liquid phase. Here, we show that this also happens at the microscale: due to localization of the contact lines at the top of the textures; the microscopic angles θ_μ at the receding edge of the droplet vary strongly as the bulk of the liquid advances, leading to critical forcing and slipping events. As a whole, due to the orientation of the three-phase contact line in the Cassie state, the contact-line motions under a droplet on a soft textured substrate involve only very limited viscous dissipation in the solid phase.

The motion of droplets also induces large deformations of the textures, mostly on the receding side. The pillars bend when the triple lines at their top are asymmetric. Their maximal deformation δ is reached on the trailing edge of the droplets, an instant before the onset of the slipping events. The deformations of soft trailing textures, although substantial (a typical scale for δ is 30 μm), do not alter the dynamics of moving droplets. To explain this surprising observation, we estimate the dissipated power due to bending of one pillar by the moving droplet. We assume that the deformation is restricted to the pillar, subjected to pure bending. The pillar of radius *r* and height *h* undergoes a deflection δ when traversed by a droplet moving at velocity *U*, with frequency $f = U/\delta$. As shown in *SI Appendix*, a typical scaling for the dissipated power during this deformation is:

$$P_{dis} \propto G''\left(\frac{U}{\delta}\right)\cdot\frac{\delta r^4}{h^3}U.$$

A millimetric droplet with volume Ω sliding down a soft textured substrate bends about 10 pillars on its receding edge. At $U = 1$ mm/s, $2\pi f \sim 1$ kHz and the loss modulus is of order 400 Pa; the total dissipated power in the viscoelastic solid is thus of the order of 10^{-11} W. This value is compared with P_η, the dissipated power in the viscous droplet,

$$P_\eta \propto \eta\Omega^{1/3}U\cdot U,$$

as described in *SI Appendix* and in ref. (29). With glycerol ($\eta \sim 1$ Pa·s), a typical scale for P_η is 10^{-9} W. The viscoelastic dissipation in the solid due to bending of the pillars is thus negligible compared to dissipation in the bulk of the droplet.

As a whole, textures screen viscoelastic braking despite their substantial deformations induced by contact with the liquid droplet. The three primary causes comprising this screening mechanism during droplet displacement are the restriction of contact-line motion to peripheral textures, the orientation of the contact lines in the Cassie state that induces pinning, precipitating rapid motion upon depinning at the receding edge or wetting initiation at the advancing edge and finally, negligible dissipation during bending of the textures. This results in a macroscopic suppression of the viscoelastic braking.

In addition to its key role in the suppression of viscoelastic braking, the geometry of the triple lines at the periphery of the droplet also induces liquid pinning on textured soft substrates. Indeed, in contrast with a flat substrate that is homogeneous and that cannot induce liquid retention in the absence of chemical heterogeneity, each texture on a soft superhydrophobic substrate is a pinning site for the liquid. The edge of the textures is sharp; as a consequence, the contact angle at its top can take multiple values without triggering motion of the triple line. For a droplet on a textured substrate inclined below the critical angle for the onset of motion α^* (sketched in Fig. 4*D*, top), θ_μ takes large values both on the receding and advancing edges of the droplet: respectively, $119 \pm 2°$ and $148 \pm 2°$, as shown in Fig. 4*D*, bottom. On the receding edge, the angle is large compared to 55°, the critical angle for rapid motion; it is also larger than the receding contact angle on the smooth substrate ($\theta_r = 87 \pm 2°$), value that needs to be exceeded for recession of the triple line on hard textured substrates (32). The contact line thus remains pinned on that edge of the droplet, while θ_μ can be very large on the advancing edge, provided the liquid does not contact the pillar on the downslope side. The microscopic contact angles at the top of the peripheral pillars have to reach critical values at both the advancing and the receding edges for the Cassie droplet to descend the substrate; the contact lines pinned by the textures anchor the liquid in place. This anchoring can lead to bending of the pillars on the receding side of the droplet, similar to what was observed on PDMS surfaces covered with slender textures (22). As was the case for the slender PDMS textures, the bending of the pillars on the receding side might explain the slight increase in the pinning strength compared to hard textured substrates. As a texture bends on the receding side, it reorients toward the liquid; compared to a rigid pillar, higher forcing is thus required for θ_μ to reach a given value.

Discussion

We report the suppression of viscoelastic braking on soft substrates by surface texturing. As a droplet of liquid is in the Cassie state, sitting on soft textures, elastocapillary deformations occur at every triple line below it. The textures at the periphery of the droplet circular imprint are the most affected by the contact with the liquid; as the contact lines at their tops are asymmetric in the horizontal plane, these textures are significantly deflected. However, all of the textures supporting the Cassie droplet exhibit a wetting ridge at their top, qualitatively similar to that observed on flat substrate with the same compliance; however, in this configuration, the deformation is parallel to the plane of the surface and it is also smaller in size than on the nontextured material. Although the presence of a ridge below a droplet on a soft substrate is usually associated with viscoelastic braking, we show that, despite the multiple ridges below a Cassie droplet, this effect is suppressed on soft textured substrates. The hallmark of this suppression is the increase by orders of magnitude of translational velocities of viscous droplets along inclined soft substrates upon the addition of textures. Whereas the main dissipation in viscoelastic braking is in the solid phase, we show that for textured substrates the dissipation occurs in the liquid.

Why are droplets moving so rapidly on soft textured substrates? First, dynamic elastocapillary deformations of the textured substrates only occur at the periphery of droplets. Second, high-speed microscopic imaging at the advancing and receding edges of the droplet shows that the triple lines move rapidly across the texture, with velocities much higher than those allowed by viscoelastic braking; they are indeed locally forced in wetting situations that strongly limit the viscous dissipation in the solid. Third, as a droplet slides over a soft textured substrate, pillars are dynamically bent, mostly on its receding edge; however, the dissipation induced in the solid is small compared to viscous dissipation in the liquid. As the viscous drag in the liquid is the main resistance to the motion of droplets, it governs the motion dynamics, as on hard substrates. Texturing soft substrates finally leads to a counterintuitive effect: it induces pinning, contrary to what is commonly observed for liquids in the superhydrophobic Cassie state on hard surfaces, where contact-angle hysteresis is much lower than on bare substrates. This can be seen most clearly in the critical inclination angle α^* required for the onset of droplet motion that is higher on soft substrates decorated with textures (even sparsely, with a low pillar density $\phi = 10\%$) than it is on smooth substrates. This effect is again a consequence of the local geometry of the contact lines at the top of the peripheral textures, where the liquid is pinned when microscopic contact angles do not reach critical values; the pillars thus act like physical defects on a material on which, when flat, pinning is absent. The pinning force is however weak, very close to that observed on hard textured substrates.

These observations open a road to the understanding of interactions between liquids and soft solids. In particular, they suggest the existence of regimes where dissipations in solids and liquids are comparable, leading to unexplored and interesting droplet dynamics. Our current methods for replication of textured silicone gels limit which aspects of textures geometry can be controlled or modified. In future investigations, it will be of great interest to see how advancements in soft surface texturing can enable the study of, for example, how more slender pillars modify droplet dynamics or how the shape of the textures alters the pinning on soft substrates. Finally, in our experiments the elastocapillary deformation size remained small compared to the size of the textures—we expect that the mechanisms described in this article will be strongly modified in the case where these two lengths are of the same magnitude.

Data Availability. All study data are included in the article and *SI Appendix*.

ACKNOWLEDGMENTS. We thank Prof. Jacco Snoeijer, Ludovic Keiser, and the LFMI laboratory at EPFL, Pierre Chantelot, Nicolas Bain, Hugo Perrin, and Lebo Molefe for helpful discussions. This work was partially financed by the Piaget Scientific Award.

1. J. F. Joanny, P. G. de Gennes, A model for contact angle hysteresis. *J. Chem. Phys.* **81**, 552–562 (1984).
2. C. G. L. Furmidge, Studies at phase interfaces. I. The sliding of liquid drops on solid surfaces and a theory for spray retention. *J. Colloid Sci.* **17**, 309–324 (1962).
3. E. B. Dussan v, On the ability of drops or bubbles to stick to non-horizontal surfaces of solids. Part 2. Small drops or bubbles having contact angles of arbitrary size. *J. Fluid Mech.* **151**, 1–20 (1985).
4. J. H. Snoeijer, E. Rolley, B. Andreotti, Paradox of contact angle selection on stretched soft solids. *Phys. Rev. Lett.* **121**, 068003 (2018).
5. B. Andreotti, J. H. Snoeijer, Statics and dynamics of soft wetting. *Annu. Rev. Fluid Mech.* **52**, 285–308 (2020).
6. A. Carré, J.-C. Gastel, M. E. R. Shanahan, Viscoelastic effects in the spreading of liquids. *Nature* **379**, 432–434 (1996).
7. T. Kajiya *et al.*, Advancing liquid contact line on visco-elastic gel substrates: Stick-slip vs. continuous motions. *Soft Matter* **9**, 454–461 (2013).
8. T. Kajiya *et al.*, A liquid contact line receding on a soft gel surface: Dip-coating geometry investigation. *Soft Matter* **10**, 8888–8895 (2014).
9. R. W. Style *et al.*, Patterning droplets with durotaxis. *Proc. Natl. Acad. Sci. U.S.A.* **110**, 12541–12544 (2013).

10. S. Karpitschka *et al*., Liquid drops attract or repel by the inverted Cheerios effect. *Proc. Natl. Acad. Sci. U.S.A.* **113**, 7403–7407 (2016).
11. S. Karpitschka *et al*., Droplets move over viscoelastic substrates by surfing a ridge. *Nat. Commun.* **6**, 7891 (2015).
12. M. E. R. Shanahan, The spreading dynamics of a liquid drop on a viscoelastic solid. *J. Phys. D Appl. Phys.* **21**, 981–985 (1988).
13. D. Long, A. Ajdari, L. Leibler, Static and dynamic wetting properties of thin rubber films. *Langmuir* **12**, 5221–5230 (1996).
14. M. Zhao *et al*., Geometrical control of dissipation during the spreading of liquids on soft solids. *Proc. Natl. Acad. Sci. U.S.A.* **115**, 1748–1753 (2018).
15. R. N. Wenzel, Resistance of solid surfaces to wetting by water. *Ind. Eng. Chem.* **28**, 988–994 (1936).
16. A. B. D. Cassie, S. Baxter, Wettability of porous surfaces. *Trans. Faraday Soc.* **40**, 546 (1944).
17. D. Richard, D. Quéré, Bouncing water drops. *Europhys. Lett.* **50**, 769–775 (2000).
18. W. Barthlott, C. Neinhuis, Purity of the sacred lotus, or escape from contamination in biological surfaces. *Planta* **202**, 1–8 (1997).
19. J. Ou, B. Perot, J. P. Rothstein, Laminar drag reduction in microchannels using ultra-hydrophobic surfaces. *Phys. Fluids* **16**, 4635–4643 (2004).
20. T. Onda, S. Shibuichi, N. Satoh, K. Tsujii, Super-water-repellent fractal surfaces. *Langmuir* **12**, 2125–2127 (1996).
21. J. Bico, C. Marzolin, D. Quéré, Pearl drops. *Europhys. Lett.* **47**, 220–226 (1999).
22. P. Papadopoulos *et al*., Wetting of soft superhydrophobic micropillar arrays. *Soft Matter* **14**, 7429–7434 (2018).
23. A. A. Dev, R. Dey, F. Mugele, Behaviour of flexible superhydrophobic striped surfaces during (electro-)wetting of a sessile drop. *Soft Matter* **15**, 9840–9848 (2019).
24. A. Lafuma, D. Quéré, Superhydrophobic states. *Nat. Mater.* **2**, 457–460 (2003).
25. R. Pericet-Camara *et al*., Solid-supported thin elastomer films deformed by micro-drops. *Soft Matter* **5**, 3611 (2009).
26. R. W. Style *et al*., Universal deformation of soft substrates near a contact line and the direct measurement of solid surface stresses. *Phys. Rev. Lett.* **110**, 066103 (2013).
27. T. Podgorski, J.-M. Flesselles, L. Limat, Corners, cusps, and pearls in running drops. *Phys. Rev. Lett.* **87**, 036102 (2001).
28. M. Reyssat, D. Quéré, Contact angle hysteresis generated by strong dilute defects. *J. Phys. Chem. B* **113**, 3906–3909 (2009).
29. T. Mouterde, P. S. Raux, C. Clanet, D. Quéré, Superhydrophobic frictions. *Proc. Natl. Acad. Sci. U.S.A.* **116**, 8220–8223 (2019).
30. R. Dufour *et al*., Zipping effect on omniphobic surfaces for controlled deposition of minute amounts of fluid or colloids. *Small* **8**, 1229–1236 (2012).
31. F. Schellenberger, N. Encinas, D. Vollmer, H.-J. Butt, How water advances on super-hydrophobic surfaces. *Phys. Rev. Lett.* **116**, 096101 (2016).
32. A. T. Paxson, K. K. Varanasi, Self-similarity of contact line depinning from textured surfaces. *Nat. Commun.* **4**, 1492 (2013).
33. A. Eddi, K. G. Winkels, J. H. Snoeijer, Short time dynamics of viscous drop spreading. *Phys. Fluids* **25**, 013102 (2013).
34. L. Chen, E. Bonaccurso, M. E. R. Shanahan, Inertial to viscoelastic transition in early drop spreading on soft surfaces. *Langmuir* **29**, 1893–1898 (2013).
35. B. B. J. Stapelbroek, H. P. Jansen, E. S. Kooij, J. H. Snoeijer, A. Eddi, Universal spreading of water drops on complex surfaces. *Soft Matter* **10**, 2641–2648 (2014).
36. A. Gauthier, M. Rivetti, J. Teisseire, E. Barthel, Role of kinks in the dynamics of contact lines receding on superhydrophobic surfaces. *Phys. Rev. Lett.* **110**, 046101 (2013).
37. M. van Gorcum, B. Andreotti, J. H. Snoeijer, S. Karpitschka, Dynamic solid surface tension causes droplet pinning and depinning. *Phys. Rev. Lett.* **121**, 208003 (2018).